ResearchGate

See discussions, stats, and author profiles for this publication at: https://www.researchgate.net/publication/230747867

Stable, microfabricated thin layer chromatography plates without volume distortion on patterned, carbon and Al2O3-primed carbon nanotube forests

Article *in* Journal of Chromatography A · August 2012

DOI: 10.1016/j.chroma.2012.07.086 · Source: PubMed

CITATIONS
28

READS
275

9 authors, including:

David Jensen
Dyno Nobel
82 PUBLICATIONS **301** CITATIONS
SEE PROFILE

Mark H Engelhard
Pacific Northwest National Laboratory
400 PUBLICATIONS **13,237** CITATIONS
SEE PROFILE

Robert C Davis
Brigham Young University - Provo Main Cam…
194 PUBLICATIONS **1,912** CITATIONS
SEE PROFILE

Matthew R Linford
Brigham Young University - Provo Main Cam…
303 PUBLICATIONS **5,257** CITATIONS
SEE PROFILE

All in-text references underlined in blue are linked to publications on ResearchGate, letting you access and read them immediately.

Available from: David Jensen
Retrieved on: 03 August 2016

Chapter 5: Stable, Microfabricated Thin Layer Chromatography Plates without Volume Distortion on Patterned, Amorphous Carbon-Primed Carbon Nanotube Forests

5.1. Abstract

Some of us recently described the fabrication of thin layer chromatography (TLC) plates from patterned carbon nanotube (CNT) forests via direct infiltration/coating of the CNTs by low pressure chemical vapor deposition (LPCVD) of silicon from SiH_4, followed by high temperature oxidation of the CNTs and Si. Herein we present an improved microfabrication process for the preparation of these TLC plates. First, a few nanometers of carbon and/or a layer of atomic layer deposition (ALD) of Al_2O_3 is deposited on the CNTs. This method of priming the CNTs for subsequent depositions appears to be new. X-ray photoelectron spectroscopy confirms the presence of additional oxygen after carbon deposition. After priming, the plates are coated by rapid, conformal deposition of an inorganic material that does not require subsequent oxidation, i.e., by fast pseudo (ψ)-ALD growth of SiO_2 via alumina catalyzed deposition of tris(*tert*-butoxy)silanol. Unlike devices described previously, faithful reproduction of the features in the masks was still observed after oxidation. A bonded, amino phase on the resulting plates showed fast, highly efficient separations of fluorescent dyes (plate heights in the range of 1.6 – 7.7 μm). Extensive characterization of the new materials by TEM, SEM, EDAX, DRIFT, and XPS is reported. A substantially lower process temperature for the removal of the CNT scaffold is possible as a result of the already oxidized materials used.

*This chapter is reproduced with permission from (David S. Jensen, Supriya S. Kanyal, Vipul Gupta, Michael A. Vail, Andrew E. Dadson, Mark Engelhard, Richard Vanfleet, Robert C. Davis, and Matthew R. Linford) *J. Chromatogr., A* **2012**, *1257*, 195-203. Copyright 2012 Elsevier B.V.

5.5. Introduction

Recently, various reports have highlighted the use of new materials in thin layer chromatography. In the early 2000s Merck introduced the UTLC (ultrathin layer chromatography) plate.[1] This device employed a thin (ca. 10 μm), monolithic silica layer with 1 – 2 μm macropores and 3 – 4 nm mesopores on a glass backing.[2, 3] However, these plates showed limited migration distances (up to ca. 3 cm) due to reduced capillary action. They also suffered from reduced sample capacity because of the limited surface area of the thin adsorbent layer. Perhaps for some of these reasons, Merck has recently stopped manufacturing these materials. Another development is the use of glancing-angle deposition (GLAD) to produce 1 – 7 μm adsorbent layers of silica.[4] This plate showed reasonable resolution and efficiencies under short development distances. Thin layer chromatography (TLC) plates based on electrospinning of nanofibrous polymers have also been described.[5] Later this same group demonstrated carbonization of electrospun polymers to form a glassy-carbon stationary phase,[6] which is similar to the commercially available porous graphitic carbon chromatographic adsorbent. Other nonsilica-based monolithic TLC plates have also been produced in an attempt to increase the separation efficiencies of large molecules.[7-9]

We recently reported a microfabrication of thin TLC plates that consisted of growth of patterned carbon nanotube forests and their subsequent infiltration with silicon via conformal, low-pressure chemical vapor deposition (LPCVD) of silane (SiH_4).[10] This study was an application to separations science of Davis and Vanfleet's seminal work on infiltrated carbon nanotube forests.[11, 12] TLC plates made in this fashion separated a test dye mixture under normal phase conditions. However, subsequent follow up studies revealed a few disadvantages to this approach. First, oxidation/conversion of silicon to silica appeared to expand and distort the features in the patterned chromatographic bed, which removed some of the advantages we had

hoped to gain through microfabrication. Such inhomogeneities in the chromatographic bed should reduce chromatographic performance by increasing the *A*-term in the van Deemter equation[13, 14] – although the van Deemter equation assumes a constant flow velocity, which clearly does not exist in the upward, capillary driven flow of a typical TLC separation, one may interpret TLC results through it.[15] Also, to the degree that feature sizes are unacceptably increased, the *C*-term of the van Deemter equation would also increase. However, because the mobile phase slows as it ascends a TLC plate, the main contribution to band broadening in TLC is due to the *B*-term in the van Deemter equation. In a few extreme cases, the fissures and channels that develop upon oxidation in the plates along the flow direction would also detrimentally affect the *B*-term by allowing increased diffusion, thus increasing the tortuosity factor of the *B*-term. In some cases, most likely as a result of these issues, irregular solvent fronts on the microfabricated TLC plates were observed. Clearly there are significant advantages to a faithful rendering/reproduction of a photolithographic mask's features in microfabrication.

Another concern with our previous study was the high temperature, ca. 850 – 1000 °C, needed to convert the LPCVD silicon to silica, which limited our choice of substrates. At elevated temperatures (above 200 °C) surface silanols (SiOH) begin to condense into siloxanes (Si-O-Si linkages), which subsequently requires their repopulation for good chromatography.[16, 17] Of course, concomitant to the oxidation of Si to SiO_2 was the desirable removal of the carbon nanotube framework, which resulted in a white TLC adsorbant material.

To overcome these issues, we developed a process that first builds on the strengths of the previous work, where advantages included: (i) the straightforward photolithographic patterning of the surface, (ii) the ease of growth of high aspect ratio, vertically aligned carbon nanotube forests, (iii) the conformal coating of these materials with an inorganic material, and (iv) the

removal of carbon nanotube templates by air oxidation. However, we explore other deposition techniques to create robust, coated, CNT forests, which upon lower temperature oxidation of the CNT framework show no distortion of features and where the resulting materials are suitable for TLC (see overview of microfabrication process in Scheme 5.1).

In particular, we focus on the priming of the CNTs with carbon and/or alumina to allow direct deposition of silica using a pseudo atomic layer deposition (ψ-ALD) process.[18] To the best of our knowledge the use of carbon as a priming layer on CNTs is new, although more extensive carbon infiltration of CNT forests has previously been reported.[19-21] Other researchers have previously attempted to prime CNTs for ALD growth, including the adsorption of NO_2 and TMA.[22] However, this approach required many NO_2 and TMA cycles prior to deposition of Al_2O_3. ALD of alumina from water and trimethylaluminum (TMA), is a straightforward and reliable ALD reaction.[22-24] The inorganic material that is finally deposited on the CNTs is already oxidized so a lower temperature can be used to burn out the underlying CNTs. An amino silane is deposited on this material, creating a bonded phase that results in rapid development times and high efficiencies for various analytes.[25] The literature contains other examples of the use of carbon nanotubes in analytical chemistry.[26, 27]

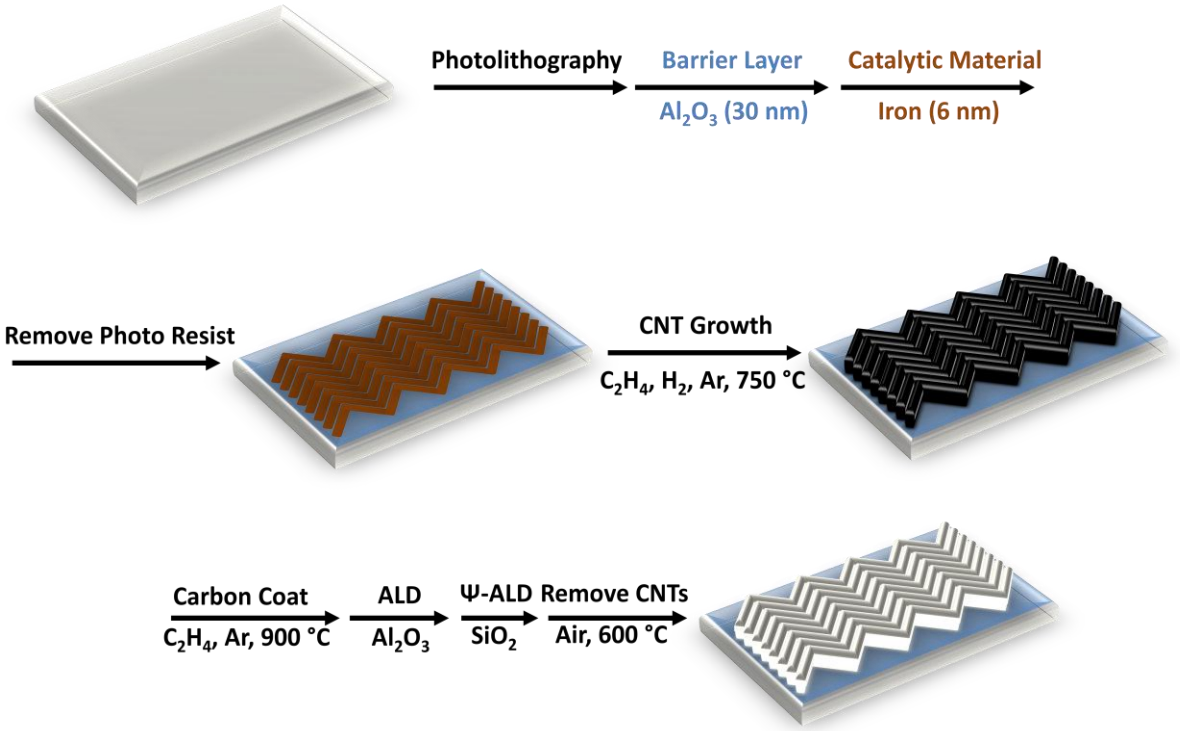

Scheme 5.1: Overview of the microfabrication process. Surfaces are photolithographically patterned. Al_2O_3 and Fe are deposited sequentially. The devices then undergo lift-off, leaving a pattern of Fe on Al_2O_3, CNT growth, coating with carbon, ALD of Al_2O_3 and pseudo-ALD of SiO_5. The material is finally heated to 600°C to remove the CNT framework.

5.3. Experimental

5.3.1. Photolithography

5.3.1.1. Dimensions of Photolithographic Features

The mask for photolithography contained patterns for four different TLC plates, all based on zig-zag geometries, 100 μm flow channels, and 90° angles between channels. Out of these four possibilities, two types of plates were used in this study: (i) a plate with 3 μm hedges and 5.65 μm flow channels, or (ii) a plate with 4 μm hedges and 4.95 μm flow channels. Both plates (i) and (ii) were used under normal phase conditions. Plate (i) was used to separate the fluorescent dyes.

5.3.1.5. Lithography and Catalytic Material Depositions

Silicon wafers (University Wafers, South Boston, MA), 4" diameter, <100>, were used as the backing material in our process. Accordingly, a thin film of photoresist, AZ-3312-F (AZ Electronic Materials USA Corp, Somerville, NJ), was spin coated onto a wafer. The resulting wafer was patterned with photolithography (Karl Suss Mask Aligner, Vermont, USA), followed by e-beam evaporation (Benton Vacuum E-beam Evaporator, Moorestown, NJ) of a thin barrier layer of alumina (35 nm), and thermal evaporation (home-built apparatus) of a few nanometers of iron (6 nm). The iron deposition was monitored using a quartz crystal device. The photoresist was then lifted off with a resist stripper (Micropsoit 1165, MicroChem, Newton, MA), leaving a pattern of Al_2O_3/Fe at the surface.

5.3.2. Microfabrication of the Thin Layer Chromatography Plate

5.3.2.1. Carbon Nanotube Growth

The photolithographically patterned wafer was loaded into a fused silica tube (22 mm ID), preheated to 200 °C in a Lindberg/Blue M tube furnace (Thermo Electron Corporation, Marietta, OH), and heated to 400 °C under flow of argon. The temperature was then raised from 400 °C to 750 ˚C in an atmosphere of hydrogen (6.67 x 10^{-6} m^3/sec), where this process reduces iron to its elemental form and simultaneously produces iron nanoparticles.[28, 29] CNTs were grown for 2 minutes at 750 ˚C to a height of ca. 50 μm with ethylene (Grade 5.0, 99.999% from Air Gas) at 1.67 x 10^{-5} m^3/sec and hydrogen (Air Gas), at 6.67 x 10^{-6} m^3/sec. The material was cooled under argon to 200 °C.

5.3.2.2. Amorphous Carbon Deposition

To improve/facilitate deposition on the CNTs, they were primed with a thin layer (4 nm) of carbon. Accordingly, the CNTs were placed in the same tube furnace used for CNT growth and the temperature was raised to 900 °C under an argon atmosphere. Carbon was then deposited at 900 °C from ethylene (5.50 x 10^{-6} m^3/sec) and argon (5.00 x 10^{-6} m^3/sec) for 45 s (deposition rate ca. 5 nm/min). After this chemical vapor deposition (CVD) of carbon the plates were cooled to 200 ˚C under argon. The thickness of the carbon was also determined on planar (100) silicon witness substrates by spectroscopic ellipsometry (M-2000D, J.A. Woollam Co., Inc., Lincoln, NE). In addition to determining the deposition rate, the deposition profile of the furnace was measured to ensure that the carbon was deposited in a uniform fashion over a uniform area (see Figure 5.1).

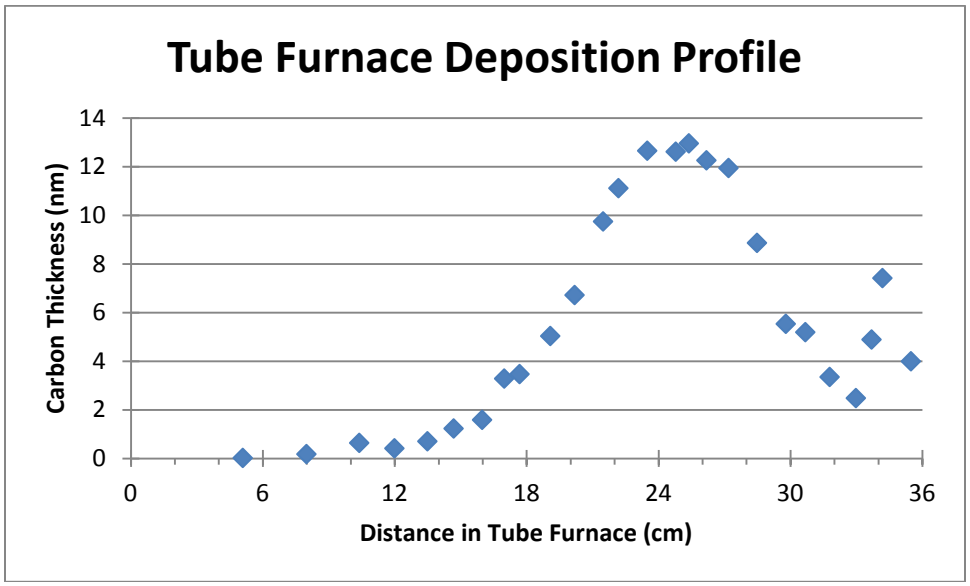

Figure 5.1. Profile for carbon deposition in our tube furnace. Deposition time was 45 s. The film thickness was determined by spectroscopic ellipsometry.

5.3.2.3. Atomic Layer Deposition (ALD) of Al_2O_3

ALD of Al_2O_3 was performed using a Cambridge Fiji F200 system (Cambridge NanoTech Inc., Cambridge, MA) from trimethylaluminum (97%, Sigma-Aldrich) and water that were cycled in an ABAB type fashion. The deposition was performed at 250 °C. Either 70 or 105 AB cycles were performed to produce film thicknesses of either 7 or 10.5 nm, respectively. Film thicknesses were monitored via spectroscopic ellipsometry with film growth of ca. 0.1 nm/cycle.

5.3.5.4. Pseudo Atomic Layer Deposition (ψ-ALD) of SiO_2

ψ-ALD of SiO_2 was also done with a Cambridge Fiji F200 system using trimethylaluminum (97%, Sigma-Aldrich) and tris(*tert*-butoxy)silanol (99.999%, Sigma-Aldrich) as precursors that were cycled in an ABAB type fashion. The deposition was performed at 235 °C. Eight AB cycles at a rate of ca. 13 nm/cycle were preformed to produce the final Al-doped SiO_2 film. Film thicknesses were monitored by spectroscopic ellipsometry.

5.3.2.4. Removal of CNTs

To produce a white material for chromatography the CNTs were removed via air oxidation. The silica coated CNTs were placed in a preheated (200°C) bench top furnace (Thermolyne 6000 Furnace, Dubuque, IA) and heated to 600 °C at 1 °C/min. The material was held at 600 °C for 17.33 h, for a total processing time of 24 h. The furnace was then cooled to 200 °C.

5.3.3. Surface modification

5.3.3.1. Rehydration of SiO_2

Because the SiO_2 material was subjected to temperatures above 200 °C, the surface needed to be repopulated with silanols.[30, 31] Surface silanol repopulation was performed with a

pH 10 NH_4OH etching solution at room temperature for 18 h. After 18 h the material was removed from solution and rinsed with deionized water to neutrality. It was dried at 120 °C prior to chromatography or APTES deposition.

5.3.3.2. Amino-Functionalization

A TLC plate was placed in a freshly prepared solution of 1% (v/v) 3-aminopropyltriethoxysilane (APTES) (≥ 98%, Sigma-Aldrich) in water-saturated toluene (≥ 99.8%, Sigma-Aldrich) and heated to 70 °C. The solution was held at this temperature for 10 min after which the TLC plate was removed and rinsed three times with methanol (≥ 99%, Sigma-Aldrich). The optical properties of Si wafers (terminated with native oxide), APTES-coated Si wafers, and carbon-coated silicon wafers were determined by variable angle spectroscopic ellipsometry (VASE) using an M-2000D instrument (J.A. Woollam Co., Inc., Lincoln, NE), which gives values of Δ and ψ from ca. 200 – 1000 nm. Ellisometric data were taken at 70° and 75° and fitted using the WVASE 32 instrument software, Version 3.635. All of the ultrathin films (the native oxide, the APTES, and the CVD carbon) were modeled using the optical constants of SiO_2 from the instrument software (sio5.jaw).

5.3.4. Material Characterization via X-ray Photoelectron Spectroscopy (XPS) and Diffuse Reflectance Infrared Fourier Transform Spectroscopy (DRIFTS)

XPS was performed on two separate instruments. XPS analysis of CNTs (n = 2) was done on a Physical Electronics Quantera Scanning X-ray Microprobe (Chanhassen, MN) at Pacific Northwest National Laboratory (PNNL) in the Environmental Molecular Sciences Laboratory (EMSL). This system uses a focused, monochromatic Al Kα X-ray (1486.7 eV)

source for excitation and a spherical section analyzer. The instrument has a 32 element multichannel detection system. A 98 W X-ray beam focused to 100 μm was rastered over a 1.3 mm x 0.1 mm rectangle on the sample. Further XPS analyses were performed using a Surface Science SSX-100 X-ray photoelectron spectrometer (serviced by Service Physics, Bend, OR) with a monochromatic Al K_α source, a hemispherical analyzer, and a take-off angle of 35°. Survey and narrow scans were recorded with an 800 μm × 800 μm spot size. The XP spectra from the SSX-100 instrument were analyzed using the ESCA Data Analysis Application software (Version: Analysis 25 V.01.02). DRIFTS was performed using a Thermo Scientific Nicolet 6700 FT-IR. Both the microfabricated material (scraped from microfabricated TLC plates) and commercially available silica (Sepax HP-Silica, 3 μm, 120 Å, Sepax Technologies, Inc., Delaware) were scanned 128 times with a resolution of 4 cm^{-1}. The spectra were analyzed using the instrument OMNIC 8.1.11 software.

5.3.5. Chromatography

5.3.5.1. Spot Application and Pre-equilbration of Thin Layer Chromatography Plate

A predetermined volume of an analyte or mixture of analytes was applied as a 3 x 0.7-0.8 mm band at the bottom of the TLC plate using a Linomat 5 spotter (CAMAG, Muttenz, Switzerland). The band was applied 5 mm from the bottom of the plate. The plate was then placed in a 10 x 10 cm twin trough chamber (CAMAG, Muttenz, Switzerland) and pre-equilibrated with the vapors of the mobile phase. After the pre-equilibration, 3 mL of the mobile phase was introduced at the bottom of the plate to commence chromatography. The TLC plate was developed over a 30 mm distance.

5.*3.5.2. Separation of a Test Dye Mixture*

Test dye mixture III solution in toluene from CAMAG (Muttenz, Switzerland) containing indophenol, ariabel red, Sudan blue II, Sudan IV, and dimethylaminoazobenzene was diluted in hexanes to produce a 1% v/v solution. A 1 µL or 3 µL volume of this diluted solution was applied to a plate, where the mobile phase was toluene (99.8%, Sigma-Aldrich), with or without 0.1% v/v triethylamine (99.5%, Sigma-Aldrich) as modifier.

5.3.5.3.1 Separation of Two Fluorescent Dyes

Eosin Y disodium salt (~85%, Sigma-Aldrich) and sulforhodamine B (75%, Sigma-Aldrich) were dissolved together in methanol to concentrations of ca. 5 x 10^{-7} M. 0.5 µL of this solution was applied and a 1:100 LiCl:methanol (LiCl, >99%, EMD, Gibbstwon, NJ) solution was used as the mobile phase.[32]

5.3.5.3.2 Separation of Four Fluorescent Dyes

Eosin Y disodium salt (~85%, Sigma-Aldrich), sulforhodamine B (75%, Sigma-Aldrich), rhodamine 6G (~95%, Sigma-Aldrich), and fluorescein sodium salt (98%, Sigma-Aldrich) were dissolved in methanol at concentrations of ca. 5 x 10^{-7} M. 0.5 µL of this solution was applied and 1:70:30 LiCl: methanol: isopropanol (isopropanol, ≥99%, Sigma-Aldrich) was used as the mobile phase

5.3.6. Visualization of Separated Dyes and Calculation of R_F , *N, and* H_{obs}

Imaging of the separated dyes was performed with a digital camera (Canon PowerShot S95, Canon USA, Inc., Lke Success, NY). The TLC plate was exposed to short wavelength UV light (254nm) (Model UVG-11 Mineralight Lamp, Ultra-Violet Products, Inc., San Gabriel, CA) for fluorescent visualization. All images were processed using ImageJ (ImageJ 1.42q, National Institutes of Health, USA).

Retention factors (R_F) were calculated with the following equation:

$$\boldsymbol{R_F = \frac{Z_o}{Z_f}} \quad (2)$$

where Z_o is the analyte migration distance from the application origin and Z_f is the distance the solvent front traveled, also from the application origin. Chromatographic efficiencies were determined by the number of theoretical plates (N) according to:

$$\boldsymbol{N = 16\left(\frac{Z_f R_f}{W}\right)^2} \quad (3)$$

where W is the width of the chromatographic band.[33] However, these values (N/m) will only be used to compare to those of Song et al.[10] Because the fluid velocity in TLC is dynamic, N is not typically used to determine chromatographic efficiency. Accordingly, observed plate heights (H_{obs}) are reported as follows:[34-38]

$$\boldsymbol{H_{obs} = \frac{\sigma^2_{chrom}}{R_F(Z_f - Z_o)}} \quad (4)$$

The value of σ^2_{chrom} in this equation is calculated from

$$\sigma^2_{obs} = \sigma^2_{chrom} + \sigma^2_{SA} + \sigma^2_{INS} \quad (5)$$

where σ^2_{obs} is the observed variance of the band after elution, σ^2_{SA} is the variance of the band at the spot application, and σ^2_{INS} is the variance of the densitometric measurement (we are not using a densitometer, so we set $\sigma^2_{INS} = 0$ in Equation 5).[34, 37, 39] The value of σ^2_{SA} was determined from the initial width of the spot at application (0.7 mm), which was taken as $5\sigma_{SA}$. Thus $\sigma^2_{SA} = 0.019_6$ mm^2 in our calculations.

5.3.7. Microscopy

SEM images were captured with an FEI Helios Nanolab 600 (Hillsboro, OR). TEM images were captured using a FEI Tecnai F20 Analytical STEM (Hillsboro, OR).

5.4. Results and Discussion

5.4.1. Conformal Coating of CNT Scaffolds

An important issue for the future manufacturing of our microfabricated TLC plates is the speed with which ca. 50 – 100 nm of conformal inorganic material can be deposited onto the CNTs. Preferably this material would be silica because silica is of primary importance in modern chromatography, cf. typical materials for TLC, HPTLC, HPLC, and UHPLC. For these reasons, we considered the rapid, pseudo ALD (ψ-ALD) process developed by Hausmann et al. that results in ca. 13 nm of silica (ψ-SiO_2) per cycle using trimethylaluminum (TMA) as a priming/catalytic layer and tris(*tert*-butoxy)silanol ($(((CH_3)_3O)_3SiOH$), (TTBS)) as the silicon dioxide precursor.[18] This deposition rate can be compared to the ca. 0.1 nm per cycle obtained in the more classical ALD deposition of SiO_2 from precursors such as $SiCl_4$ and H_2O.[40]

Accordingly, we attempted to grow ψ-SiO_2 directly onto patterned CNT forests using the Hausmann process, and significant growth was observed. However, the resulting thin ψ-SiO_2

films on CNTs lacked conformality and usually showed a large number of pearl-like features (see Figure 5.2a). This lack of conformal growth was expected to affect the plates' mechanical stability. Indeed, after removal of the CNTs via air oxidation, the plates were submerged in water and immediate failure/delamination was observed. It seemed unlikely that these devices could act as acceptable substrates for thin layer chromatography.

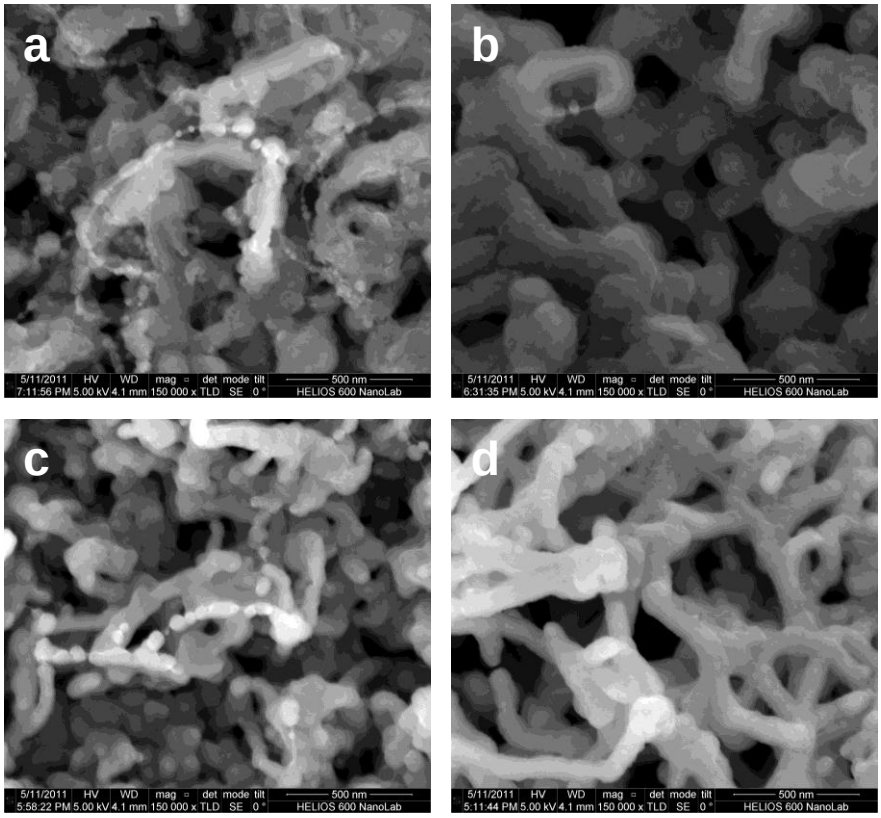

Figure 5.2. Scanning electron micrographs of materials for TLC prepared under various conditions. At least some pearl-like nucleation/growth appears in the first three of the micrographs: (a) CNT-ψ-SiO_2(8), (b) CNT-a-C(4 nm)-ψ-SiO_2(8), (c) CNT-Al_2O_3(70)-ψ-SiO_2(8), and (d) CNT-a-C(4 nm)-Al_2O_3(70)-ψ-SiO_2(8). The unitless numbers in parentheses signify the number of ALD cycles completed.

The pearl-like growth observed in the direct deposition of ψ-SiO_2 from TMA and TTBS appeared to be the result of an insufficient number of nucleation sites on the CNTs, which are quite chemically inert. In this situation an appropriate adhesion promoter, which might increase the number of nucleation sites on the CNTs, might allow more conformal growth to take place. As noted above, there are previous reports of the filling/infiltration of CNT forests with carbon.[19, 20, 41] However, in contrast to these studies, we believed that only a very thin layer, perhaps only a few nanometers, might be sufficient to significantly increase the number of nucleation sites available for subsequent ALD. To the best of our knowledge, this method for chemically activating CNTs is new. We hypothesized that these nucleation sites would be oxygen-containing moieties at defects in the carbon layer. Accordingly, a few nanometers of carbon was deposited onto CNTs using ethylene diluted in argon at 900 °C. The resulting carbon layers showed good conformality and even some measure crystallinity, as indicated by the texture of their transmission electron microscopy (TEM) images (Figure 5.3).

X-ray photoelectron spectroscopy (XPS) of unprimed and carbon coated CNTs was also performed. Multiple XPS scans of multiple unprimed CNT forests showed the material to be 100% carbon (n=6). In contrast, XPS of carbon coated CNTs showed the presence of oxygen (0.80 ± 0.11 atom% O, 99.20 ± 0.11 atom% C from four scans of four different CNT forests, see Figures 5.4).

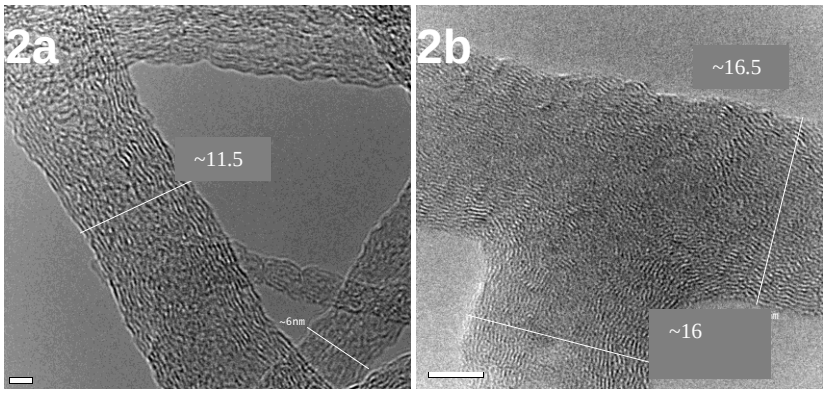

Figure 5.3. (a) TEM image of as-grown CNTs (scale bar 2 nm) (b) TEM image of CNTs coated with amorphous carbon (45 s deposition time) (scale bar 5 nm).

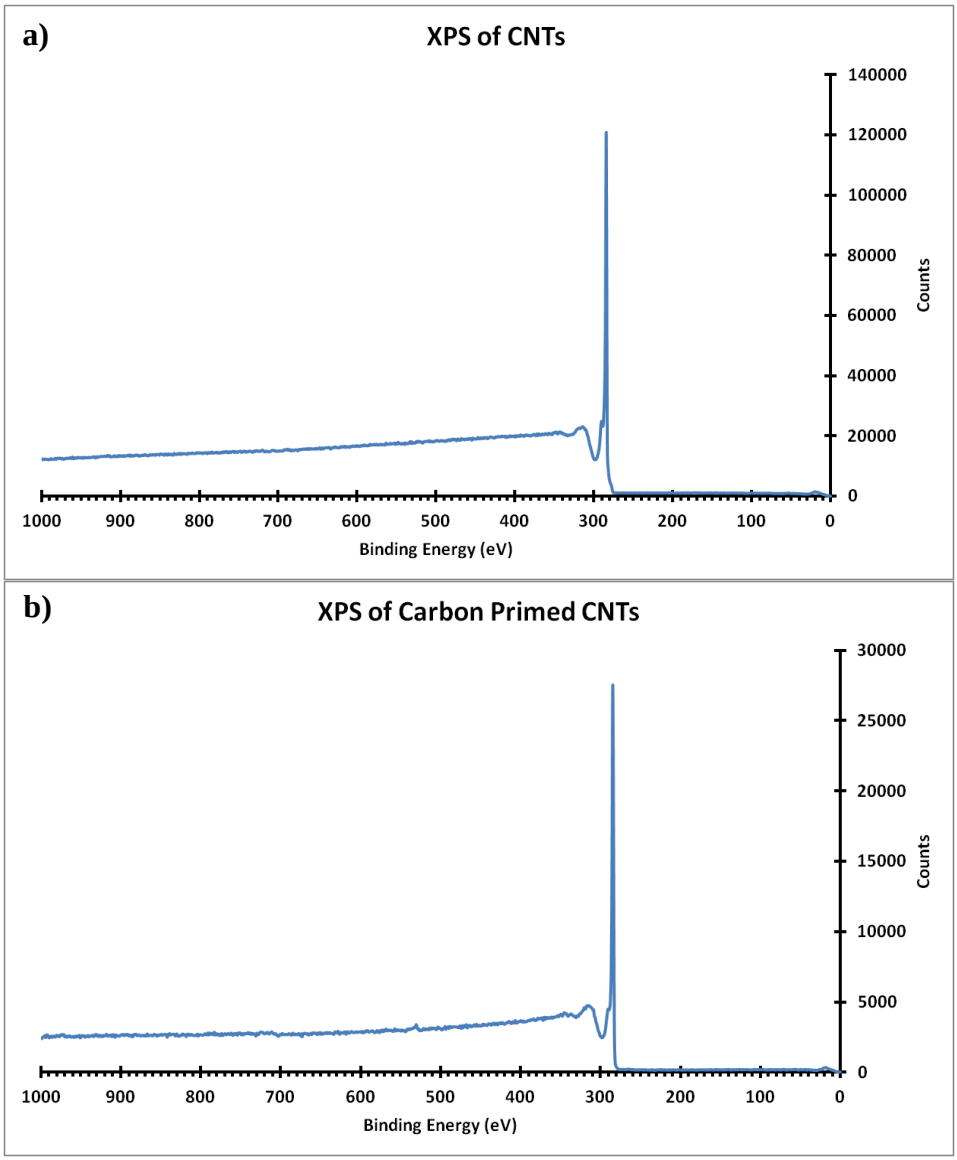

Figure 5.4. a) XPS survey spectum of as grown CNTs. No element except carbon (at ca. 285 eV) is present. Oxygen would appear at ca. 530 eV. b) XPS survey spectrum of carbon-primed CNTs. The spectrum shows both carbon at ca. 285 eV and a small oxygen signal at ca. 530 eV.

This increase in oxygen should increase the number of nucleation sites available for ALD, especially given the highly reactive nature of trimethylaluminum.

To explore whether these few nanometers of carbon might improve ALD or ψ-ALD on CNTs, and to show that these plates might indeed exhibit the desired stability and chromatographic properties, four types of depositions were performed on patterned CNT forests using different combinations of carbon (C), Al_2O_3 (deposited in a 'true' ALD process), and ψ-SiO_2: (i) CNT-ψ-SiO_2(8), (ii) CNT-C(4 nm)-ψ-SiO_2(8), (iii) CNT-Al_2O_3(70)-ψ-SiO_2(8), and (iv) CNT-C(4 nm)-Al_2O_3(70)-ψ-SiO_2(8), where the number in parentheses after 'Al_2O_3' and 'ψ-SiO_2' refers to the number of ALD or pseudo ALD cycles, one cycle referring to the introduction of both precursors for each process. Both these and also the deposition mentioned below (same as deposition (iv) but with more Al_2O_3 ALD cycles) were made on patterned nanotube forests. Each of these four depositions was performed three times, from start to finish, in separate fabrications. After deposition of carbon, Al_2O_3, and/or fast (ψ-ALD) deposition of SiO_2, the coated materials were oxidized to remove both the CNT framework and the carbon priming layer. In contrast to our previous work,[10] it was no longer necessary to convert the Si to SiO_2 so the nanotubes and carbon layer could be burned out at a much lower temperature (ca. 600 °C). Finally, the plates were visually inspected for whiteness, where a whiter plate points to a greater deposition of inorganic material, as it hides the darker silicon substrate. As expected, the CNT-ψ-SiO_2(8) plates visually showed the least amount of deposition (they were the darkest) and all of them failed a water immersion test, showing immediate delamination/removal of the layer. The CNT-C(4 nm)-ψ-SiO_2(8) plates (Figure 5.2b) showed more SiO_2 deposition, but ca. 50% of them failed the water immersion test. The CNT-Al_2O_3(70)-ψ-SiO_2(8) plates performed about as well as the CNT-carbon(4 nm)-ψ-SiO_2(8) plates, with one plate completely passing and about half of

another plate passing the immersion test (Figure 5.2c). The best performing substrates contained both CVD carbon and Al_2O_3 (Figure 5.2d); they showed the greatest deposition of inorganic material (greatest whiteness) and ca. 2.5 of 3 plates passed the immersion test (only part of one plate failed). This synergistic effect of both carbon and alumina to create a stable structure is attributed to the introduction of oxygen at defect sites on carbon, followed by sufficient growth of Al_2O_3 by ALD at these sites so that strong nucleation would occur in subsequent ψ-SiO_2 growth – note that exposure/deposition of trimethylaluminum is the first setp in ψ-SiO_2 growth. Thus, it appeared that at this point we had a nearly viable process for fabricating TLC plates with features that did not swell or expand upon oxidation. Figure 5.5 shows SEM micrographs of portions of TLC plates prepared with our original method, showing some distortion of the features, and with this newer approach showing straight, undistorted features. More stable materials, which withstood the water immersion test after oxidation, were next prepared by increasing the number of Al_2O_3 ALD layers. TEM/STEM analysis of the resulting CNT-C(4 nm)-Al_2O_3(105)-ψ-SiO_2(8) materials showed the expected sequential encapsulation of the CNTs and carbon with Al_2O_3 and ψ-SiO_2 (see Figure 5.6), (See also Figure 5.7 for other TEM images.)

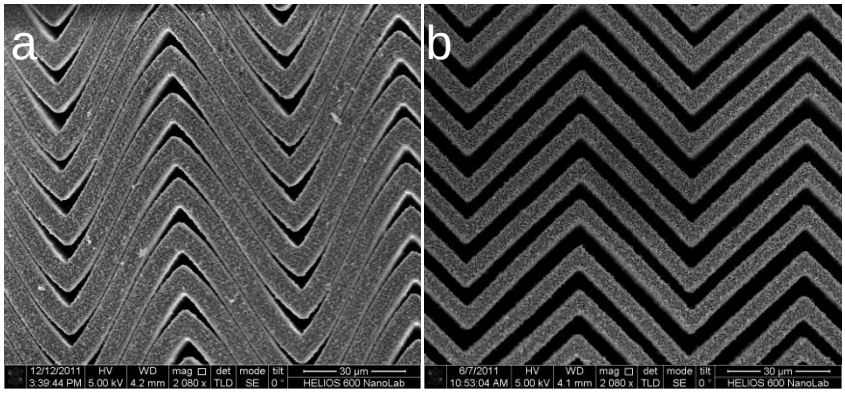

Figure 5.5. SEM images of (a) a TLC plate prepared via the method of Song et al.[10] (b) a TLC plate prepared by the method described within this manuscript. Both plates were made from the same lithography mask, plate (ii). Note that the flow direction for TLC in these devices would be from left to right, or right to left.

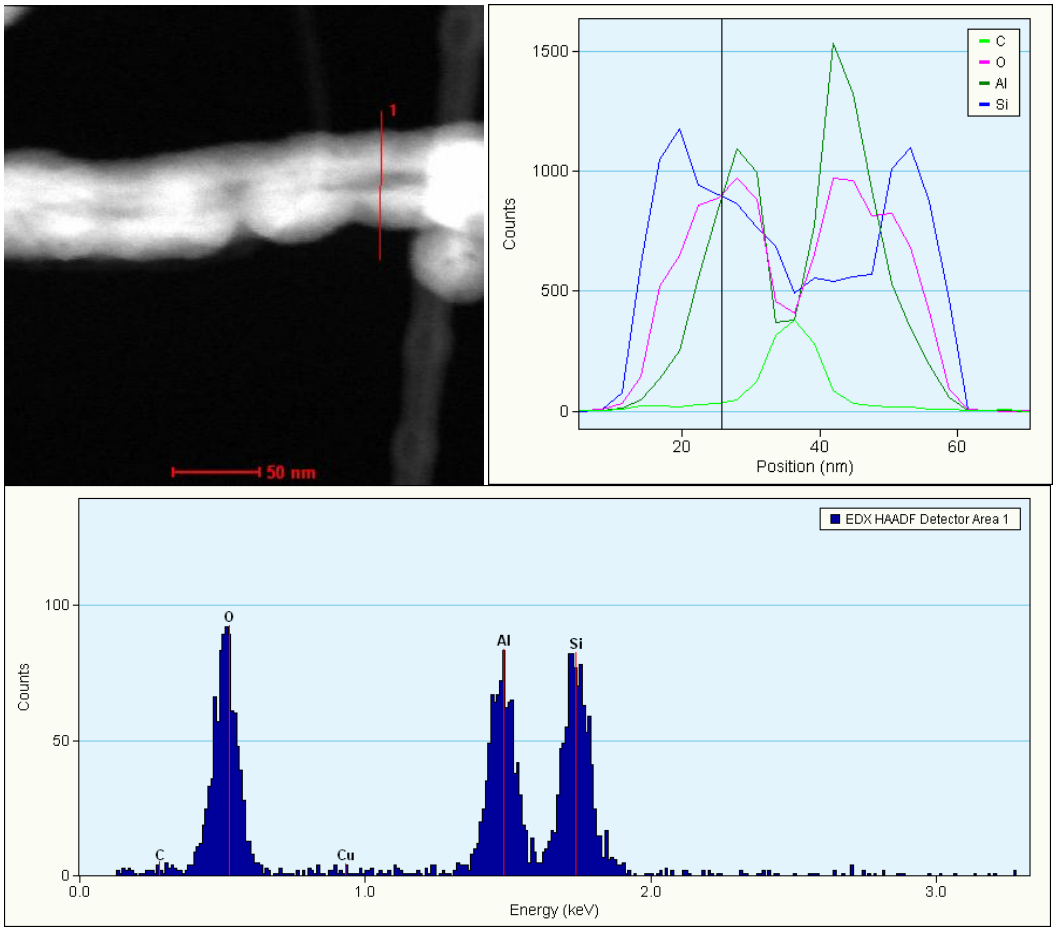

Figure 5.6. STEM of the CNT-C(4nm)-Al_2O_3(105)-ψ-SiO_2(8) assembly. STEM shows the expected presence of carbon, aluminum, oxygen and silicon, with carbon at the center of the assembly, followed by aluminum, and then silicon.

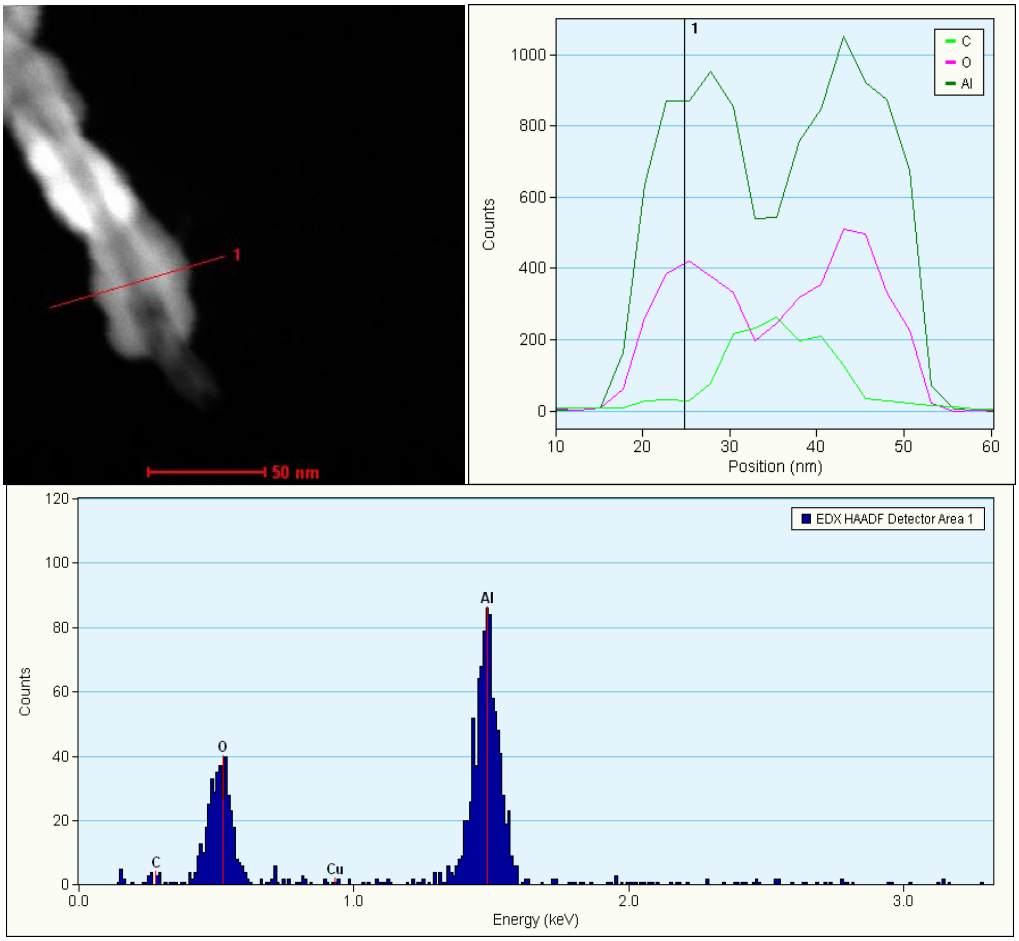

Figure 5.7. STEM of alumina-coated CNT. A carbon coated CNT is located in the center of the feature and is encapsulated with Al_2O_3.

5.4.2 Separations on Microfabricated-Thin Layer Chromatography (M-TLC) Plates

TLC was then performed on the better (CNT-C(4nm)-Al_2O_3(105)-ψ-SiO_2(8)) plates. However, because temperatures as low as 200 °C are known to remove silanol (SiOH) groups from silica,[42] and because appropriate densities of SiOH groups are essential for good chromatography,[31] the plates were first hydrated via a literature method that consisted of (i) immersion in a pH 10 NH_4OH solution for 18 hours, and (ii) rinsing with water to neutrality.[31] TLC of a CAMAG test dye mixture was then performed under normal phase conditions with the recommended mobile phase (toluene). The results were mixed. First, the run times for the plates were short, which of course is positive: ca. 30 s development times for 30 mm development distances. Second, all of the analytes in the test mixture generally showed substantial streaking except the fastest moving analyte, which appeared as a tight band, with an observed plate height (H_{obs}) of 4.1 μm (ca. 77 000 theoretical plates per meter (N/m)) for the plate (ii) geometry and H_{obs} of 5.6 μm (ca. 100 000 N/m) for plate (i) at moderate retention factor (R_F) values of ca. 0.6 (See Figure 5.8). These results suggested the presence of strongly adsorbing sites that interact to a greater extent with the more polar (more strongly retained) analytes in the test mixture.

Metal impurities, including aluminum, are well known to create strongly adsorbing sites in silica that deleteriously affect chromatography. Indeed, one of the significant advances in liquid chromatography over the past few decades has been the development of the so-called Type B silica, which, in contrast to the older Type A, has extremely low levels of metal impurities.[43, 44] So while in theory our plates should be entirely covered by silica, one possible source of strongly adsorbing sites could be aluminum from the ψ-ALD deposition of SiO_2, i.e., alumina from $Al(CH_3)_3$ is the catalyst that begins each deposition cycle.

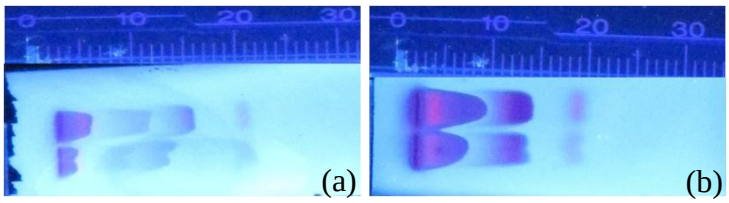

Figure 5.8. Separation of a CAMAG test dye mixture on two microfabricated TLC plates with different geometries. (a) 4 µm hedges and 4.95 µm flow channels (CNT-C(4nm)-Al_2O_3(105)-ψ-SiO_2(8), plate (ii)), and (b) 3 µm hedges with 5.65 µm flow channels (CNT-C(4nm)-Al_2O_3(105)-ψ-SiO_2(8), plate (i)). Both separations were performed over 30 mm with development times of ca. 30 s. Plates were visualized under 254 nm light. For the fastest moving analyte in (a): R_F = 0.63 with an efficiency (H_{obs}) of 5.6 µm (100 000 N/m), and in (b): R_F = 0.55 with an efficiency (H_{obs}) of 4.1 µm (77 000 N/m).

Accordingly, X-ray photoelectron spectroscopy (XPS) was performed on a CNT-C(4 nm)-Al_2O_3(70)-ψ-SiO_2(8) plate to determine whether any aluminum was present in the upper ca. 5 - 10 nm of the SiO_2 film, which is the approximate probe depth of the technique. A negative signal (no Al by XPS) would indicate that the aluminum was entirely covered with a thick layer of silica. A small positive signal would be ambiguous – the Al might be covered with a moderately thick film of SiO_2 or it might be near enough to the surface to create highly acidic/adsorptive sites. XPS showed ca. 2 atom% Al on the TLC material. Interestingly, less Al (0.2 atom%) was found on a planar ψ-SiO_2 film, which suggested that the deposition of ψ-SiO_2 on the curved nanotubes was not quite the same as on a planar substrate, and that this difference in geometry may change the distribution of Al in the plate.

In addition to XPS, diffuse reflectance infrared Fourier transform spectroscopy (DRIFT) was performed on our materials, along with a commercially available standard silica material produced for HPLC. This study was motivated by Köhler et al., who showed that highly adsorptive silicas with highly acidic/isolated silanols that show poor chromatographic performance have peak maxima for silanols at or greater than 3740 cm^{-1}, while silicas that show better chromatographic performance show a maximum below this value, which corresponds to associated/more closely spaced/hydrogen bonded silanols.[31] The DRIFT analysis of our material gave a silanol peak position of 3740.5 cm^{-1}, suggesting the presence of at least some highly adsorptive sites, while the commercial silica standard gave a value of 3739.9 cm^{-1}.

Thus, chromatographic, XPS, and DRIFT analyses suggested that strongly adsorbing sites were present in our stationary phase/support and that these may be due to aluminum. To further probe this issue, a small amount (0.1%) of triethylamine (TEA) was added to the mobile phase. TEA is a well-known modifier to mobile phases for liquid chromatography on the older

Type A silica materials, where its function was to interact strongly with isolated silanols/strongly adsorbing sites.[45-47] TEA had two effects on our TLC separations. First, it changed the chromatographic characteristics of the mobile phase, i.e., it strengthened it, which resulted in higher R_f values for the analytes. Indeed, the analytes largely ran together with R_f values of ca. 0.8. But more importantly, the addition of TEA eliminated streaking on the plates. The results from these experiments are consistent with the presence of strongly adsorbing sites on our plates. With this information, our next goal was to find a chemical reagent that might permanently bind to/cover up the strongly adsorbing sites on our TLC plates. And because TEA, an amine, seemed to reduce or eliminate the effects of strongly adsorbing sites, hydrated TLC plates were reacted with an amino silane: 3-aminopropyltriethoxysilane (APTES). This is the first demonstration of a bonded phase on one of our microfabricated TLC plates. An advantage of APTES in silane deposition is that, due to its primary amine, it catalyzes its own condensation.[48] APTES deposition was inferred from planar shards of silicon that were placed in the solution, which showed increases in thickness of 1.6 ± 0.1 nm by spectroscopic ellipsometry. The advancing and receding water contact angles on these planar surfaces were 46.3 ± 1.7° and 8.4 ± 1.0°, respectively, which is consistent with literature results.[49, 50] XPS further confirmed APTES deposition, showing a small but noticeable nitrogen signal (N1s:Si2p ratio of 2:25) for APTES-coated TLC plates. No such signal was present on the plate prior to deposition of the silane. TLC of two fluorescent dyes was first attempted on a somewhat defective APTES-functionalized CNT-C(4 nm)-Al_2O_3(70)-ψ-SiO_2(8) plate. Fortunately, both compounds appeared to separate under these conditions, or at least to be separable, albeit with same distortion. A CNT-C(4 nm)-Al_2O_3(105)-ψ-SiO_2(8) plate was then functionalized with APTES, and the separation of the fluorescent dyes was attempted as before. This time a baseline separation of the dyes was

observed in 1:08 min over a 30 mm distance (see Figure 5.5). This same separation was performed on a commercially available amino-HPTLC plate under the same conditions. Comparing the solvent front migration times between the two TLC plates (microfabricated vs. HPTLC) our plates ran 3 times faster (amino-HPTLC development time: 3:26 min).

The green spot in Figure 5.9, which is probably most representative of the separation, showed an R_F value of 0.85 with H_{obs} of 7.7 μm (ca. 85,000 N/m). The orange spot, which migrated further and with an R_F of 0.94, was probably focused by the solvent front so the corresponding value of H_{obs} (6.6 μm or 89,000 N/m) may be inflated. This two component separation was promising and was reproduced on three separate TLC plates. It was apparent that surface functionalization with APTES rendered a material that was more suitable for chromatography. Accordingly, we attempted to separate a four-component fluorescent dye mixture: eosin Y disodium salt, sulforhodamine B, rhodamine 6G and fluorescein sodium salt, using a 1:70:30 LiCl: methanol: isopropanol mobile phase. Figure 5.10 shows the separation of these dyes on an APTES-functionalized TLC plate in a rather short period of time (1:52 minutes) over a 30 mm development distance.

This latest separation showed improved efficiencies over the previous separations, which may be attributed to a reduction in the mobile phase migration rate due to a more viscous mobile phase, and which may have allowed the separation to occur at a better mobile phase velocity. The efficiencies obtained in this separation ranged from 1.6 to 5.8 μm (200,000 to 270,000 N/m) (more specifically H_{obs} of 5.8 μm, 1.6 μm, 1.9 μm, 5.1 μm at R_F values of 0.79, 0.86, 0.89, and 0.94, respectively). The separated dyes appeared as symmetrical bands, which would again be consistent with APTES covering highly adsoptive sites on the ψ-ALD deposited SiO_5.

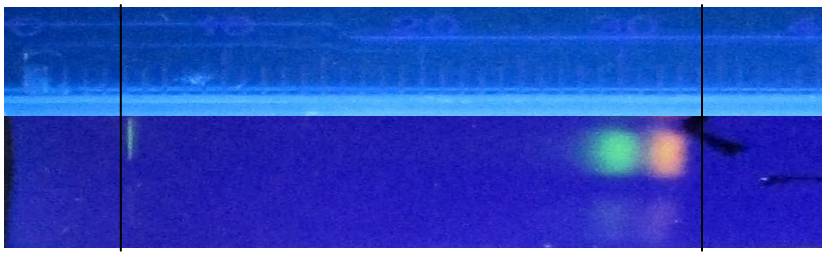

Figure 5.9. Separation of two fluorescent dyes (eosin Y disodium and sulforhodamine B) over a 30 mm run distance using a 1:100 LiCl:methanol mobile phase. The analyte concentration in the lower track is ca. 10% of the concentration of the analytes in the upper track. The fluorescent image was captured under 254 nm light.

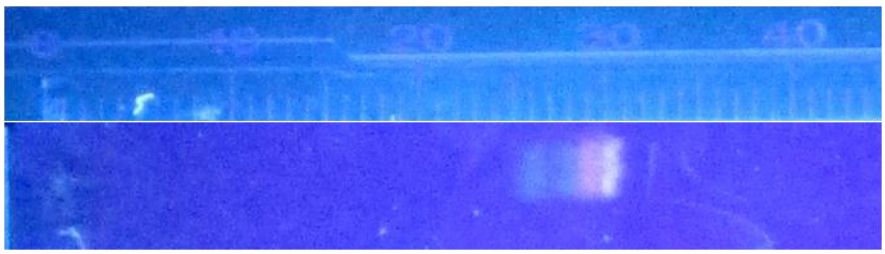

Figure 5.10. Separation of four fluorescent dyes (eosin Y disodium salt, sulforhodamine B, rhodamine 6G and fluorescein sodium salt) using a 1:70:30 LiCl:methanol:isopropanol mobile phase. The development occurred over a 30 mm distance in 1:52 minutes. The fluorescent image was captured under 254 nm light.

A comparison of these results to a commercially available amino-phase HPTLC plate showed that these TLC plates were ca. 6 times more efficient and ca. 4 times faster. Thus, microfabricated TLC plates allow for both extremely efficient separations and increased speed of analysis.

The use of ALD type reactions to coat CNTs for the construction of a chromatographic medium has proven to give more efficient chemical separations when compared to the original work done by some of us.[10] The maximum number of theoretical plates per meter (N/m) previously obtained was ca. 75,000 N/m. The process described within this document produced a chromatographic medium that gave a maximum of 270,000 N/m (1.6 μm), a significant improvement.

5.5. Conclusions

Microfabricated TLC plates were constructed from CNT-patterned surfaces. The CNTs were coated with silica, the chromatographic material, via pseudo-atomic layer deposition.[18] The use of an adhesion layer of carbon and ALD of Al_2O_3 allowed for the construction of silica-coated TLC media that were mechanically robust. After surface functionalization with APTES to cover strongly adsorptive sites, two different test dye mixtures were successfully separated. Separations occurred in short periods of time with high efficiencies.

5.6. References

1. Stevenson, R., Chapter 12 Instrumentation. In *Journal of Chromatography Library*, Heftmann, E., Ed. Elsevier: 2004; Vol. Volume 69, pp 469-518.

2. Hauck, H.; Bund, O.; Fischer, W.; Schulz, M., *J. Planar Chromatogr.--Mod. TLC* **2001,** *14* (4), 234-236.

3. Hauck, H.; Schulz, M., *Chromatographia* **2003,** *57* (0), S313-S315.

4. Bezuidenhout, L. W.; Brett, M. J., *J. Chromatogr., A* **2008,** *1183* (1-2), 179-185.

5. Clark, J. E.; Olesik, S. V., *Anal. Chem.* **2009,** *81* (10), 4121-4129.

6. Zewe, J. W.; Steach, J. K.; Olesik, S. V., *Anal. Chem.* **2010,** *82* (12), 5341-5348.

7. Bakry, R.; Bonn, G. K.; Mair, D.; Svec, F., *Anal. Chem.* **2006,** *79* (2), 486-493.

8. Han, Y.; Levkin, P.; Abarientos, I.; Liu, H.; Svec, F.; Fréchet, J. M. J., *Anal. Chem.* **2010,** *82* (6), 2520-2528.

9. Urbanova, I.; Svec, F., *J. Sep. Sci.* **2011,** *34* (16-17), 2345-2351.

10. Song, J.; Jensen, D. S.; Hutchison, D. N.; Turner, B.; Wood, T.; Dadson, A.; Vail, M. A.; Linford, M. R.; Vanfleet, R. R.; Davis, R. C., *Adv. Funct. Mater.* **2011,** *21* (6), 1132-1139.

11. Hutchison, D. N.; Morrill, N. B.; Aten, Q.; Turner, B. W.; Jensen, B. D.; Howell, L. L.; Vanfleet, R. R.; Davis, R. C., *J. Microelectromech. Syst* **2010,** *19* (1), 75-82.

12. Moulton, K.; Morrill, N. B.; Konneker, A. M.; Jensen, B. D.; Vanfleet, R. R.; Allred, D. D.; Davis, R. C., *J. Micromech. Microeng.* **2012,** *22* (5), 055004.

13. Billen, J.; Desmet, G., *J. Chromatogr. A* **2007,** *1168* (1-2), 73-99.

14. John H, K., *J. Chromatogr. A* **1999,** *831* (1), 3-15.

15. Reich, E.; Schibli, A., *High-performance thin-layer chromatography for the analysis of medicinal plants*. Thieme Medical Publishers, Inc.: New York, 2007.

16. Van Le, T.; Ross, E. E.; Velarde, T. R. C.; Legg, M. A.; Wirth, M. J., *Langmuir* **2007,** *23* (16), 8554-8559.

17. Bergna, H. E.; Roberts, W. O., *Colloidal silica: fundamentals and applications*. Taylor & Francis Group: Boca Raton, 2006; Vol. 131.

18. Hausmann, D.; Becker, J.; Wang, S.; Gordon, R. G., *Science* **2002,** *298* (5592), 402-406.

19. Gong, Q.-m.; Li, Z.; Li, D.; Bai, X.-d.; Liang, J., *Solid State Commun.* **2004,** *131* (6), 399-404.

20. Gong, Q.-m.; Li, Z.; Bai, X.-d.; Li, D.; Liang, J., *Compos. Sci. Tochnol.* **2005,** *65* (7-8), 1112-1119.

21. Kleckley, S.; Chai, G. Y.; Zhou, D.; Vanfleet, R.; Chow, L., *Carbon* **2003,** *41* (4), 833-836.

22. Cavanagh, A. S.; Wilson, C. A.; Weimer, A. W.; George, S. M., *Nanotechnol.* **2009,** *20* (25), 255602.

23. Dillon, A. C.; Ott, A. W.; Way, J. D.; George, S. M., *Surf. Sci.* **1995,** *322* (1-3), 230-242.

24. Ott, A. W.; Klaus, J. W.; Johnson, J. M.; George, S. M., *Thin Solid Films* **1997,** *292* (1-2), 135-144.

25. Tleugabulova, D.; Zhang, Z.; Chen, Y.; Brook, M. A.; Brennan, J. D., *Langmuir* **2003,** *20* (3), 848-854.

26. Valcárcel, M.; Cárdenas, S.; Simonet, B. M., *Anal. Chem.* **2007,** *79* (13), 4788-4797.

27. Merkoçi, A., *Microchim. Acta* **2006,** *152* (3), 157-174.

28. Mattevi, C.; Wirth, C. T.; Hofmann, S.; Blume, R.; Cantoro, M.; Ducati, C.; Cepek, C.; Knop-Gericke, A.; Milne, S.; Castellarin-Cudia, C.; Dolafi, S.; Goldoni, A.; Schloegl, R.; Robertson, J., *J. Phys. Chem. C* **2008,** *112* (32), 12207-12213.

29. Esconjauregui, S.; Fouquet, M.; Bayer, B. C.; Ducati, C.; Smajda, R.; Hofmann, S.; Robertson, J., *ACS Nano* **2010,** *4* (12), 7431-7436.

30. Bergna, H. E.; Roberts, W. O., *Colloidal silica: fundamentals and applications*. Taylor & Francis Group: Boca Raton, 2006; Vol. 131.

31. Köhler, J.; Kirkland, J. J., *J. Chromatogr. A* **1987,** *385* (0), 125-150.

32. Wako Pure Chemical Industries Ltd. NH2 Silica Gel 60F254 Plate-Wako. http://www.wako-chem.co.jp/english/labchem/pdf/NH2_TLC_Plate.pdf.

33. Poole, C. F.; Poole, S. K., *Anal. Chem.* **1989,** *61* (22), 1257A-1269A.

34. Poole, S. K.; Poole, C. F., *J. Chromatogr. A* **2011,** *1218* (19), 2648-2660.

35. Poole, C. F., *The Essence of Chromatography*. 2003.

36. Bertsch, W.; Hara, S.; Kaiser, R. E.; Zlatkis, A., *Instrumental HPTLC*. Huethig, 1980.

37. Spangenberg, B.; Poole, C. F.; Wiens, C., *Quantitative Thin-Layer Chromatography: A Practical Survey*. Springer: New York, 2011.

38. Prosek, M.; Golc-Wondra, A.; Vovk, I., *J. Planar Chromatogr.* **2001,** *14*, 100.

39. Poole, C. F., *J. Planar Chromatogr.* **1988,** *1*, 373.

40. Sneh, O.; Wise, M. L.; Ott, A. W.; Okada, L. A.; George, S. M., *Surf. Sci.* **1995,** *334* (1-3), 135-152.

41. Li, X.; Ci, L.; Kar, S.; Soldano, C.; Kilpatrick, S. J.; Ajayan, P. M., *Carbon* **2007,** *45* (4), 847-851.

42. Bergna, H. E., Colloid Chemistry of Silica: An Overview. In *Colloidal Silica Fundamentals and Applications*, Bergna, H. E.; Roberts, W. O., Eds. Taylor & Francis Group: Boca Raton, 2006; Vol. 131, pp 9-35.

43. Kirkland, J. J.; Dilks Jr, C. H.; DeStefano, J. J., *J. Chromatogr. A* **1993,** *635* (1), 19-30.

44. Stella, C.; Rudaz, S.; Veuthey, J.; Tchapla, A., *Chromatographia* **2001,** *53* (0), S113-S131.

45. Park, J.; Ryu, Y.; Lim, H.; Lee, H.; Lee, Y.; Jang, M.; Suh, J.; Carr, P., *Chromatographia* **1999,** *49* (11), 635-642.

46. Hill, D. W.; Kind, A. J., *J. Liq. Chromatogr.* **1993,** *16* (18), 3941-3964.

47. Dolan, J. W., *LCGC Eur.* **2003,** *September*, 2-4.

48. Asenath Smith, E.; Chen, W., *Langmuir* **2008,** *24* (21), 12405-12409.

49. Zeng, X.; Xu, G.; Gao, Y.; An, Y., *J. Phys. Chem. B.* **2010,** *115* (3), 450-454.

50. Zhang, F.; Sautter, K.; Larsen, A. M.; Findley, D. A.; Davis, R. C.; Samha, H.; Linford, M. R., *Langmuir* **2010,** *26* (18), 14648-14654.